John von Neumann Institute for Computing


# Proteins as Molecular Machines: Force Probe Simulations

Helmut Grubmüller

published in

*Computational Soft Matter: From Synthetic Polymers to Proteins, Lecture Notes,*
*Norbert Attig, Kurt Binder, Helmut Grubmüller, Kurt Kremer (Eds.),*
*John von Neumann Institute for Computing, Jülich,*
*NIC Series, Vol.* **23***, ISBN 3-00-012641-4, pp. 401-422, 2004.*



http://www.fz-juelich.de/nic-series/volume23

# Proteins as Molecular Machines: Force Probe Simulations

**Helmut Grubmüller**

Theoretical and Computational Biophysics Department,
Max-Planck-Institute for Biophysical Chemistry,
Am Fassberg 11, 37077 Göttingen, Germany
*E-mail: hgrubmu@gwdg.de*

Many proteins are molecular "nano-machines", which perform their biological function via well-coordinated structural transitions. In most cases, these transitions occur on much slower time scales than those accessible to conventional molecular dynamics techniques. Force probe simulations provide a powerful means to overcome this limitation and thus to get insight into the atomistic mechanisms that underly biological functions. This chapter provides a basic introduction into this method. It further sketches a simple non-equilibrium statistical mechanics treatment that shows how to connect the results of force probe simulations with atomic force microscopy experiments. Finally, the method is applied to study mechanical energy transfer steps in $F_1$ ATP synthase, probably the smallest rotary motor on earth.

## 1 Introduction

Proteins are macromolecules, consisting of many thousands of atoms. Virtually all biomolecular tasks in the call are carried out by proteins. Examples are the maintenance of structures (collagen), enzymatic catalysis, chemical signal transduction (immunoglobulines and hormones), DNA transcription and duplication, chemico-mechanical energy conversion (motor proteins) transport across membranes, and the degradation of dispensable or degenerated proteins. Other functions are the transport or filtering of small molecules (ion pumps, aquaporins), molecular recognition (antibodies), photosynthesis, sensoring (e.g. rhodopsin), or the triggering of membrane fusion[1]. Traditionally, changes in the Gibbs free energy are the central concept to follow and describe these processes. More recently, with the advent of single molecule force probe experiments and the perception of proteins as "molecular machines", the application and detection of targeted forces open a new route — both experimentally and on the theory side — to protein function[2]. The theoretical aspects and appropriate simulation techniques are the subject of this chapter.

## 2 Protein Structure and Dynamics

Contrary to most other polymers, proteins adopt under native conditions (typically aqueous solvent at $20 - 40^{\circ}$C and neutral *pH*) a well defined spatial structure[3], i.e., the (average) position of each single atom of the protein is well-defined. This remarkable fact allows to measure all the atomic positions by X-ray crystallography or nuclear magnetic resonance (NMR) spectroscopy. The Protein Data Bank[4] currently (2004) archives more than 20 000 such atomically resolved protein structures.

Very early experiments have suggested periodic structural elements in proteins. W.T. Astbury (a scholar of W.L. Bragg), e.g., observed characteristic patterns in X-ray scattering experiments on hairs already in the thirties. Remarkably, these patterns changed upon

stretching of the hair, and Astbury referred to the two respective structures as "$\alpha$" and "$\beta$". This was the first direct observation of a structural transition in a protein. The similarly regular helical structure of DNA discovered by Watson and Crick twenty years later led to the general belief that all biological macromolecules exhibit a simple and regular structure.

When John Kendrew determined the structure of myoglobin[5] — a small muscular oxygen transport protein — in 1958, its extraordinary complexity and lack of regularity came, therefore, to many as a surprise. Kendrew remarked: "Perhaps the most remarkable features of the molecule are its complexity and lack of symmetry. The arrangement seems to be almost totally lacking in the kind of regularities which one instinctively anticipates."

From a physical/chemical point of view, the irregular — but highly ordered — protein structure is in fact not easy to explain. In solution, essentially all other polymers adopt a huge number of different, usually quickly interchanging structures ("random coil"). Even polypeptides with random amino acid sequence (as opposed to the specific sequences of proteins selected by evolution) typically do not fold into well defined structures. Thus, the question of which physical principles govern the self-organized folding of proteins into their native, three-dimensional structure, is still unresolved. This is demonstrated from the very fact that, still, it is not possible to predict this structure solely from the (genetically determined and unique) amino acid sequence ("primary structure") — although the protein structure is, under native conditions, fully determined by the sequence. This long standing problem is called "folding problem", and by many considered the "holy grail" of theoretical molecular biophysics.

From an evolutionary point of view, however, it would be very surprising *not* to find well-defined protein structures: As soon as one accepts that the quite complex functions carried out by proteins (such as enzymatic catalysis, signal transduction, motor function, ion pumping and filtering and many more) require "gadgets" with at least similarly complex blueprints — i.e., if the analogy of a "nano-machine" holds — then one must indeed expect proteins to exhibit a high degree of structural and dynamic organization, built up from components the properties and motions of which are tailored towards the desired function.

Thus, a crucial selection criterium for proteins is apparently to fold (under physiological conditions) reliably, reproducibly, and in a self-organized manner into unique spatial structures. (As is often the case in biology, there are exceptions. Some proteins seem to perform their task without any well-defined spatial structure). From this picture it follows that already quite minute perturbations of protein structures, of the physico/chemical properties of single amino acids within a protein, or their intramolecular interactions, can compromise or even destroy the proper functioning of a particular protein. The large number of hereditary diseases and specific forms of cancer, which originate from modifications of single base pairs in the genes (and, therefore, from the exchange of a single amino acid within the encoded protein), demonstrates that this is in fact the case. The picture of a carefully aligned "molecular machine" is further supported by the observation that already minute changes in temperature, *pH*, or salt concentration, can destroy protein structure and function.

These examples also illustrate the essential role of collective structural transitions for protein function, so-called conformational transitions[6]. These differ from the thermal high-frequency vibrations, which fall into the picosecond range, in that they occur on much slower time scales, from nanoseconds to seconds. The opening and closing of ion channel

proteins in nerve cells is an example for such a functional conformational transition. It is characterized by millisecond rates and can be observed via an electric current through the channel by patch-clamp measurements[7–9] on single proteins. Other examples are so-called allosteric effects (e.g., in hemoglobin), which are realized by conformational transitions, and induced fit motions upon ligand binding, e.g., of a antigen to an antibody. Last but no least we mention the elementary steps of motor proteins for muscle contraction, which also represent conformational transitions.

Functional processes in proteins occur on a large variety of different time scales, and so does protein dynamics and conformational dynamics, which covers a wide hierarchy of dynamical processes: the high frequency part of the thermal fluctuations of single atoms around their average position is characterized by reciprocal frequencies of several ten to several hundred femtoseconds; collective motions of smaller groups of atoms range up to several ten picoseconds. Larger structural changes occur on a hierarchy of time scales ranging from nanoseconds to hours. There is a convincing amount of experimental and theoretical evidence for "hierarchical substates"[6] for protein conformations, which are linked by conformational transitions on a wide range of time scales[10]. These conformational dynamics apparently is a feature specific to proteins and other systems of comparable complexity[11].

The highly ordered, but heterogeneous structure of proteins in combination with the broad range of non-separating time scales in protein dynamics renders the application of established concepts of many body physics extremely difficult; work in this direction, therefore, is a challenging field in theoretical physics. Most current approaches, however, aim at describing and predicting quite general properties of protein dynamics of protein folding, and functional processes of specific proteins are typically not accessible.

Accordingly, the explicit, atomically resolved molecular dynamics simulation of the protein of interest is still to be considered the only reliable theoretical description. The lack of more elegant treatments has a high price: such protein dynamics simulations are computationally extremely demanding and, therefore, with presently available hardware (e.g., Linux clusters), restricted to relatively small simulations systems (several $100,000$ atoms) and, most severely, to short time scales of several tens of nanoseconds. Nevertheless, the method is now widely and successfully employed for a large number of biological processes that fall into this category, and has yielded a large number of correct predictions and insights into protein function at the atomic level[12]. The general method of molecular dynamics simulation is introduced by Mike P. Allen in a separate chapter of this book; here we shall, therefore, focus on the aspects specific for protein dynamics simulation.

## 3 Protein Dynamics Simulations

Molecular dynamics simulations compute the motion of every single atom within the simulation system (e.g., a protein solvated in physiological solvent (Fig.1, left), which is determined by the interaction forces (Fig.1, right) between all the $n$ atoms of the system. Typically, these forces are described by a "force field" $V(\mathbf{x}_1, \ldots, \mathbf{x}_n)$, which serves to compute a trajectory $\{\mathbf{x}_i(t_j)\}_{i=1\ldots n; j=0\ldots N}$ via the (classical) Newtonian equations of motion. This trajectory specifies the position $\mathbf{x}_i$ of each single atom in the system within a (discretized) period of time, $t_0 = 0$, $t_1 = \Delta t$, $t_2 = 2\Delta t$, $\ldots$, $t_N = N\Delta t$, for $N$ so-called integration steps. From such a trajectory one can subsequently calculate the observables of interest,

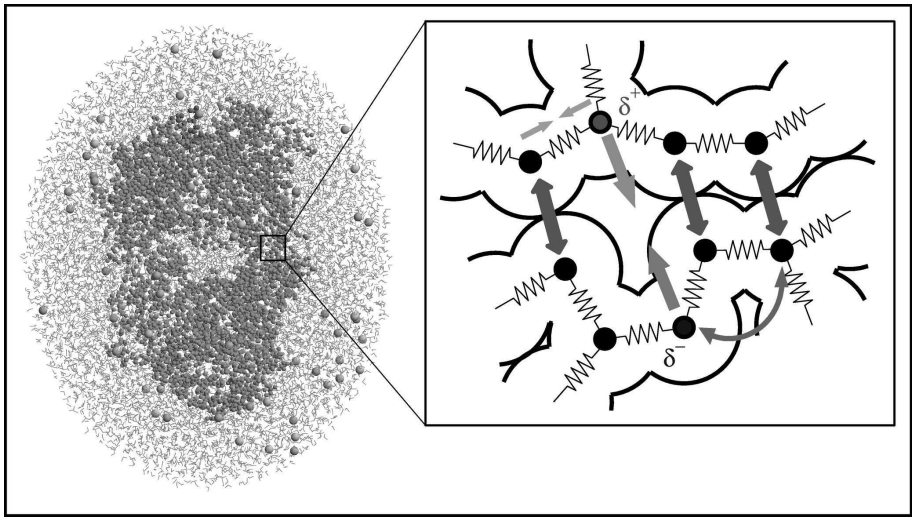


Figure 1. Left: A typical protein dynamics simulation system comprises a protein (dark grey atoms) solvated in water (light grey; only the O–H-bonds are shown). Salt ions (sparse light grey atoms) have been added to the aqueous solvent. Right: The inset shows part of the system, together with selected interatomic forces (e.g., chemical binding forces, Coulomb forces between atoms that carry partial charges, Pauli repulsion, van der Waals attraction) which determine the molecular motion.

often via averages.

Back in 1955, Fermi and co-workers have calculated numerically the motions of a one-dimensional chain of coupled anharmonic oscillators[13]. This first molecular dynamics simulation already highlights an essential aspect of the method: The simulation suggested an unexpected periodicity of the solution, and only with this simulation result in mind the authors could come up with a stringent derivation of a remarkable, non-linear partial differential equation (the Kortweg-de Vries-equation) for the continuum limit. Very similarly, the purpose of today's protein dynamics simulations is two-fold: first, to compute and predict observables; second, and often even more importantly, to provide the necessary insights and ideas which stimulate further studies.

Two years later, Alder and Wainwright studied systems of hard, two-dimensional discs[14]. For the first time, Rahman and Verlet used a more realistic interaction potential to study correlated motions and memory effects in liquid argon[15,16] and, later, also in water[17]. The duration of those simulations was about 10 ps. The classical approximation of the nuclear motion also allowed to treat reactive scattering reactions in molecular beams such as the H+$H_2$-reaction[18]; these calculations served to compare the simulation results with transition state theories.

To facilitate the refinement of protein structure models to data from x-ray scattering experiments on protein crystals, and building upon earlier works on n-alkanes, cyclo-alkanes, and polypeptides[19], Shneior Lifson suggested in 1969 to construct an interaction force field also for proteins[20]. Combining infrared spectra, geometrical information from amide crystals, and quantummechanical calculations, a number of self consistent force field was developed and applied during the subsequent years.

The availability of these protein force fields finally triggered the first simulations of a protein[21,22] (in gas phase, i.e., without surrounding solvent) for $10\,\mathrm{ps}$. The static structure of hemoglobin, e.g., did not reveal the pathway via which oxygen atoms reach the binding site, which is deeply buried within the protein. The mentioned protein dynamics simulations provided the solution to this problem by suggesting that the thermal motion of the protein creates transient pathways for the oxygen molecule. This was the first of many subsequent examples for the relevance of protein dynamics at the atomic level for protein function[23].

Increased computer power and improved algorithms extended accessible system sizes and time scales. In 1998, the conformational dynamics of a small protein was simulated over one microsecond[24], requiring half a year of computer time on a 512 processor Cray T3E supercomputer. By joint use of donated computer time from more than $100,000$ PCs located all over the world, recently a large number of trajectories could be accumulated for the study of protein folding processes, covering a total of several hundred microseconds[25].

For medium sized systems of about $100,000$ atoms, currently simulations of several 10 nanoseconds durations are feasible at justifiable computational cost[26,27]. One can estimate from this number that a further increase of computer power by a factor of about $10^4$ will be required to cover most biochemical elementary reactions such as enzymatic catalysis or the transport of an ion across the membrane by ion pump proteins. For protein folding simulations, a $10^6$- to $10^8$-fold increase would be required. Assuming that the annual increase by a factor of $1.6$ observed for the past 35 years continues into the future, these aims could be reached within 20 to 40 years. Today, 27 years after the first molecular dynamics simulation of a protein, and despite the impressive $10^5$-fold increase of computer power since then, the limited system size and, particularly, limited simulation lengths are our main obstacle in the attempt to derive the biochemical processes in proteins that enable our life from first principles physics laws.

## 4 Force Fields for Protein Dynamics

The forces between the atoms of a solvated macromolecule (Fig. 1 left) are diverse (inset, right). Chemical binding forces, symbolized by springs, enforce equilibrium distances or angles between chemically bound atoms (small arrows). Pauli repulsion forces (dark arrows) prevent atoms from moving through each other. Long ranged interactions, particularly electrostatic forces (light arrows) between partially charged atoms ($\delta^+$, $\delta^-$) contribute substantially to the stability of protein structures and dominate the slow conformational dynamics. Hydrogen bonds, e.g., are mainly of electrostatic origin and only to a lesser extent a quantummechanical effect, and contribute significantly to the stability of $\alpha$-helices and $\beta$-sheets[28].

All three forces (and several more, which are not discussed here) determine the three-dimensional structure of a protein as well as the motion of each single atom and, therefore, have to be considered in protein dynamics simulations. As mentioned before, this is achieved via the force field $V$, which describes the influence of the electronic dynamics on the motion of the nuclei. Most force fields are composed of empirically motivated interaction terms. Construction, parameterization, and testing of a force field is a challenging task, and substantial efforts will be required to further improve their accuracy.

Since the seventies, a number of force fields for biomolecules and, specifically for

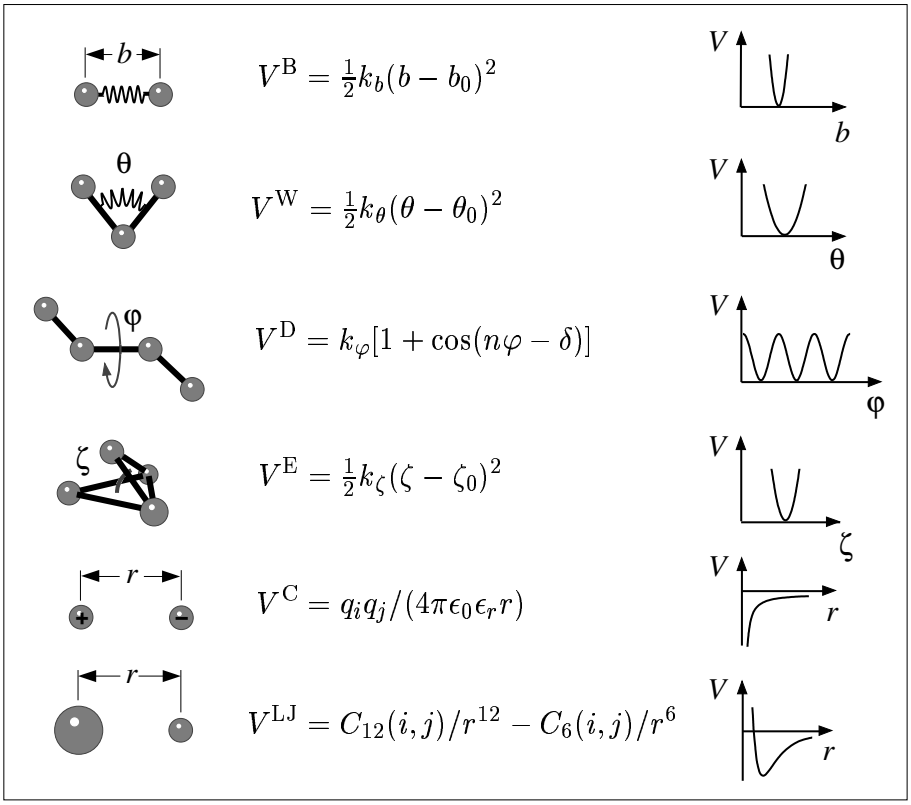


Figure 2. Interaction contributions to a typical force field (graphics adapted from Ref. 29). Bond stretch vibrations are described by a harmonic potential $V^{\mathrm{B}}$, the minimum of which is at the equilibrium distance $b_0$ between the two atoms connected by chemical bond $i$ [cf. eq. (1); the indices $i$, $j$ etc. are not shown in the Figure]. Bond angles and out-of-plane angles are also described by harmonic potential terms, $V^{\mathrm{W}}$ and $V^{\mathrm{E}}$, where $\Theta_0$ and $\zeta_0$ denote the respective equilibrium angles. Dihedral twists are subjected to a periodic potential $V^{\mathrm{D}}$; the respective force coefficients are denoted by $k$'s with appropriate indices. Non-bonded forces are described by Coulomb interactions, $V^{\mathrm{C}}$, and Lennard-Jones potentials, $V^{\mathrm{LJ}} = V^{\mathrm{P}} + V^{\mathrm{vdW}}$, where the latter includes the Pauli repulsion, $V^{\mathrm{P}} \sim r^{12}$, and the van der Waals interaction, $V^{\mathrm{vdW}} \sim -r^6$.

proteins and DNA/RNA have been developed. Well known and widely used are, e.g., CHARMM, GROMOS96, AMBER, and OPLS. Figure 2 shows interaction terms from which these force fields are typically composed. They describe interactions that arise from covalent chemical bonds as well as non-covalent interactions,

$$V = \sum_{\substack{\text{bonds}\\ i}} V_i^{\mathrm{B}} + \sum_{\substack{\text{bond}\\ \text{angles } j}} V_j^{\mathrm{W}} + \sum_{\substack{\text{dihedral}\\ \text{angles } k}} V_k^{\mathrm{D}} + \sum_{\substack{\text{extraplanar}\\ \text{angles } l}} V_l^{\mathrm{E}} + \sum_{\substack{\text{atom pairs}\\ r,s}} (V_{r,s}^{\mathrm{C}} + V_{r,s}^{\mathrm{P}} + V_{r,s}^{\mathrm{vdW}}) \,. \qquad (1)$$

Covalent forces arise from changes of the length of chemical bonds ('B') and of the angle between two bonds ('W'), from twisting chemical bonds ('D'), and deviations of aromatic

carbon atoms from their in-plane positions ('E'). As non-covalent interactions the Coulomb interaction ('C'), the Pauli repulsion ('P') and the van der Waals interaction ('vdW') are included; the latter two are conveniently described by a Lennard-Jones-potential.

Many important details of protein dynamics simulations cannot be described and discussed at this basic level. Those include the treatment of the system boundaries or, alternatively, their periodic continuation, the "freezing" of fast bond vibrations to mimic their quantum mechanical character, the proper placement of salt ions in the vicinity of the protein, the treatment of protonable residues, simulations in canonical thermodynamic ensembles via appropriate coupling to heat and pressure baths, the treatment of non-poler hydrogen atoms through "compound atoms", pros and cons of explicit vs. implicit treatments of hydrogen bonds, the set-up of a simulation system using structures derived from x-ray crystallography and the problem of sufficiently long equilibration of the system, the implicit (or, in part, explicit) description of electronic polarizability, the efficient computation of the long-ranged Coulomb forces and the parallelization of the respective algorithms, as well as the proper choice of numerical integrators for the solution of the Newtonian equations of motion. Excellent reviews articles have been published on these topics[30–32]; for a full in-depth treatment, the reader is referred to the books of Gunsteren, Weiner and Wilkinson[33].

## 5 Force Probe Simulations[a]

The recent years have seen dramatic improvements in single molecule experiments, particularly atomic force microscopy (AFM) methods, which triggered the force probe simulation technique described in this section.

In the experiments, the cantilever of the AFM microscope is used as a piconewton force sensor (Fig. 3 top right). The cantilever can be positioned to sub-nanometer accuracy, and its deflection — measuring the applied force — is detected via a laser beam with equally high precision.

Figure 3 (top left) illustrates the experiment, in which a ligand (biotin, light grey) is forced by the cantilever to leave the specific binding pocket of the receptor (streptavidin, dark grey). A polymer linker connects the proteins (with empty binding pockets) with a surface (left) as well as several biotin molecules with the tip of the cantilever (right). As the cantilever approaches the surface, several biotin/streptavidin complexes form, which dissociate one after the other upon subsequent retraction of the cantilever. Occasionally, one *single* complex remains intact until the very end of the experiment, in which case the force required to dissociate this last complex can be measured from the jump of the deflection of the cantilever to zero.

By repeating the experiment several hundred times one obtains a histogram of dissociation forces (Fig. 3 bottom right). Its maximum denotes the most probable dissociation force, in the shown example ca. 270 pN. This is the force that the non-covalent binding interaction between ligand and receptor can withstand at the time scale set by the experiment (typically milliseconds to seconds).

In a similar manner molecular forces have been measured recently for a a number of systems. One example is the force generated by single motor proteins[36] which is used to

[a] Parts of this Section are adapted and translated from Ref. 34.

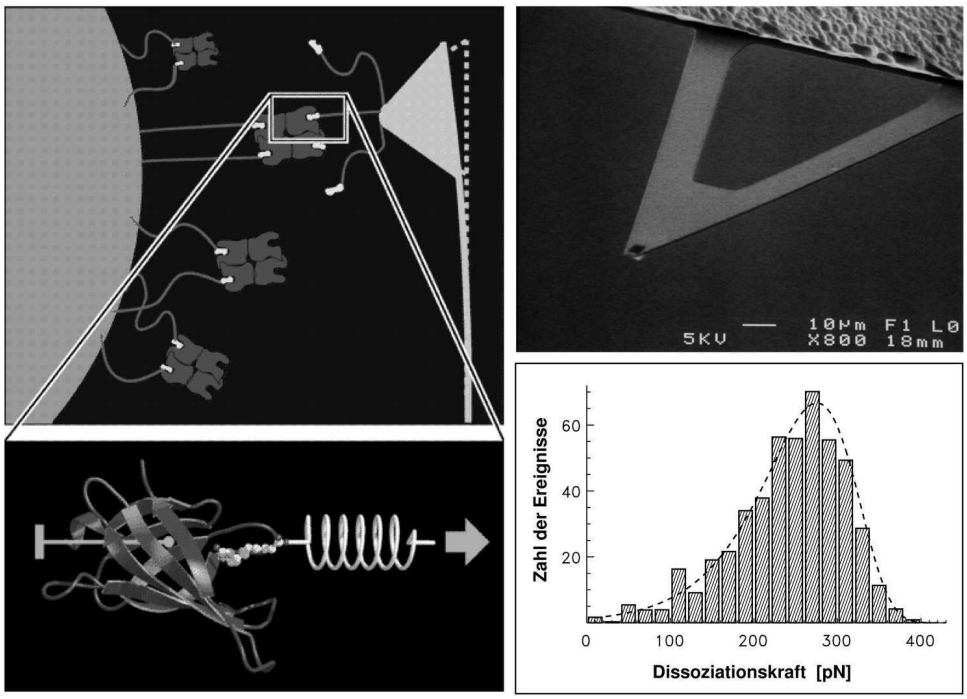


Figure 3. Top left: Principle of single molecule AFM experiments (see text); top right: electron microscopy picture of an AFM cantilever (picture kindly provided by Nanoscope); bottom left: simulation of single molecule AFM experiments (see text); bottom right: typical force histogram obtained from a series of single molecule unbinding experiments and fit to theory (dashed) [adapted from Rief et al.[35]].

drive muscle contraction or to transport intracellular vesicles along filaments. An other one is the force generated by DNA polymerase upon transcription along the DNA primer[37].

However, in those experiments, the underlying atomistic dynamics and interactions that generate the observed forces could not be observed, which is the main motivation to simulate these experiments by means of protein dynamics simulations (Fig. 3 bottom left). To that aim, and modeling the effect of the cantilever, an additional harmonic "pulling potential",

$$V(\mathbf{R}_i, t) = \tfrac{1}{2}k[(\mathbf{R}_i - \mathbf{R}_i^0) \cdot \hat{\mathbf{n}} - vt]^2 \tag{2}$$

is included within the molecular force field such that it acts on that particular atom $i$ of the ligand molecule, which in the real experiment is covalently connected to the cantilever via the polymer linker. This ensures that in the simulation the atom is subjected to the same force as in the experiment. In the Figure, this pulling potential is symbolized by a spring. The normalized vector $\hat{\mathbf{n}}$ denotes the direction of pulling, and $\mathbf{R}_i^0$ the position of atom $i$ at the start of the simulation. As can be seen from eq. (2), the minimum of the pulling potential (i.e., the equilibrium position of atom $i$) is subsequently moved with constant velocity $v$ away from the binding pocket (arrow).

To avoid drift of the protein, the center of mass of the protein (consisting of $n_p$ atoms

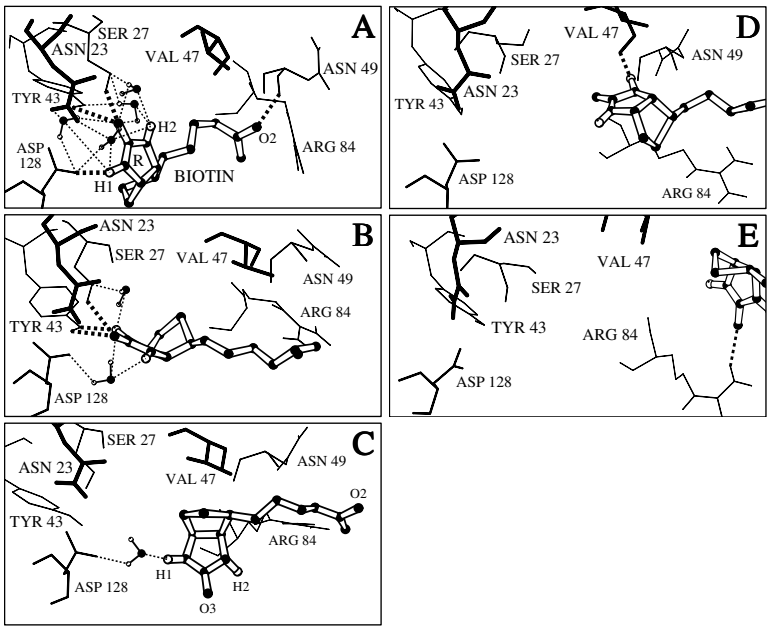


Figure 4. Snapshots of enforced dissociation of a biotin molecule (white, thick contours) from the streptavidin binding pocket (only the few relevant residues of the binding pocket are shown as stick-models). Hydrogen bonds are shown as bold dashed lines, few of the many water bridges with thin, dotted lines. The simulation length is one nanosecond; during this time the biotin molecule is moved by about one nanometer. (Adapted from Ref. 38).

with positions $\mathbf{R}_i$, $i = 1 \ldots n_p$) is kept in place at $\mathbf{R}_{\rm fix}$ by a second harmonic (but stationary) potential,

$$V_{\rm fix}(\mathbf{R}_1, \ldots, \mathbf{R}_{n_p}) = \tfrac{1}{2} k_{\rm fix} \left[ \mathbf{R}_{\rm fix} - \frac{1}{n_p} \sum_{i=1}^{n_p} \mathbf{R}_i \right]^2 , \tag{3}$$

with suitable spring coefficient $k_{\rm fix}$. This ensures that the protein is free to undergo internal motions, such as induced-fit motions upon ligand unbinding, and that it can adopt to the pulling direction by rotations — as in the real experiment —, but prevents translational motions.

These force probe AFM simulations of enforced dissociation allowed one to compute dissociation forces, which agreed well with those measured in the AFM experiments. In such comparisons one has to carefully take into account the fact that the AFM measurements and the force probe simulations are carried out at quite different time scales, namely milliseconds versus nanoseconds. Therefore, in order to compare the respective dissociation forces, the computed force has to be re-scaled to the measured ones, e.g., for the simplest case using eq. (13), as will be described below.

Figure 4 shows a detailed model of streptavidin/biotin dissociation derived from force probe simulations, highlighting the sequence and type of stretching and subsequent rupture of single non-covalent bonds between the ligand and the receptor[38,39]. These complex sequence of localized rupture events give rise to a complex "force profile" (Fig. 5), i.e., the

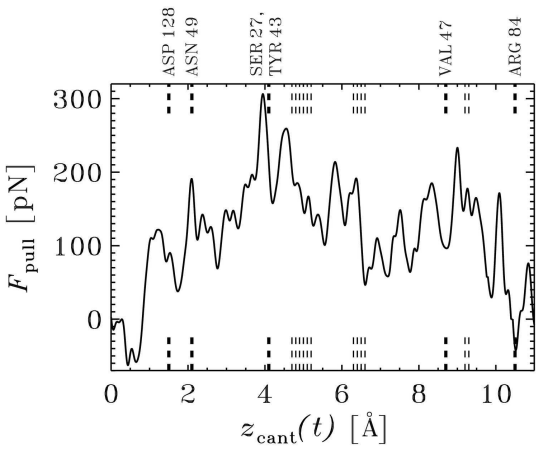


Figure 5. Force exerted onto the biotin ligand during enforced dissociation ("force profile"). A large number of local force maxima can be seen, each of which can be attributed to the rupture of single non-covalent bonds like hydrogen bonds or water bridges. The bold dashed lines at the top denote the respective residues, which are also shown in Fig. 4. the thin dashed lines denote rupture of water bridges (adapted from Ref. 38).

exerted force plotted during the simulation,

$$F_{\rm pull} = \hat{\mathbf{n}} \cdot \nabla V(\mathbf{R}_i, t) = k\, \hat{\mathbf{n}} \cdot [(\mathbf{R}_i - \mathbf{R}_i^0) \cdot \hat{\mathbf{n}} - vt]\,. \tag{4}$$

This type of force probe simulations, also called "steered molecular dynamics", is now widely used, e.g., to elucidate at the atomic level the structural changes that are induced by mechanically unfolding proteins like titin[40,41] or by stretching various other polymers[42–44], and to explain the measured forces in terms of intramolecular interactions. For more extended review, we would like to refer the reader to Refs. 35, 45.

## 6 Simple Non-Equilibrium Statistical Mechanics of Enforced Dissociation[b]

For complex systems like proteins, the measured and computed dissociation or unfolding forces vary with the time scale at which the process is enforced to occur. Usually, the forces increase with shorter time scales, i.e., increasing loading rates. For thermodynamic equilibrium, such time scale dependency should not appear; hence, the underlying processes are likely to proceed far from equilibrium. This observation motivated the development of non-equilibrium theories of enforced unbinding reactions[47,48,39,49–51]. One of these shall be sketched here.

We assume an effective free energy $G(x)$ along a (one-dimensional) reaction coordinate $x$ (Fig. 6, solid bold line), e.g., the distance between the center of mass of the ligand and the one of the receptor, which governs the dissociation reaction.

As sketched in the two Figures, the bound state (left minimum) is separated from the dissociated state (right) by a more or less structured energy barrier (global maximum). The

[b] Parts of this section are translated from Ref. 46.

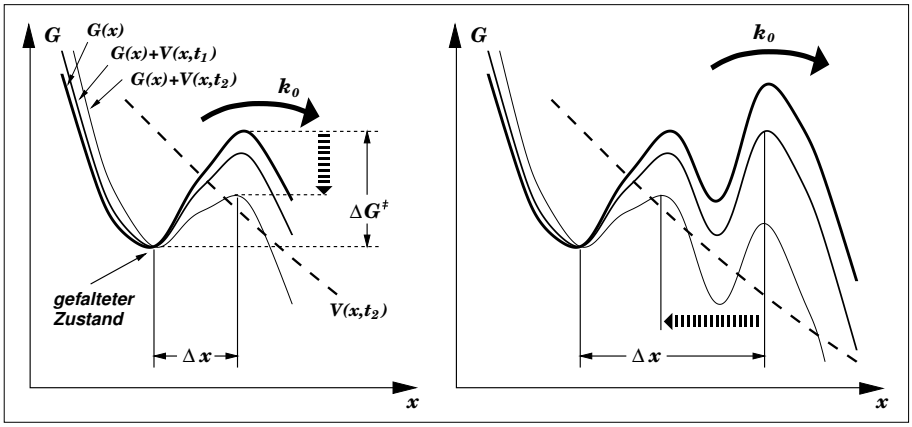


Figure 6. Time dependent Gibbs free energy in force probe experiments and simulations. A time-dependent potential $V(x,t)$ describes the force exerted by the cantilever and modifies the unperturbed energy landscape $G(x)$. As a result, the barrier that determines the spontaneous dissociation rate $k_0$ (black arrow) is reduced (left: dashed vertical arrow). For a more complex energy landscape (right), also the dissociation length $\Delta x$ (dashed horizontal arrow), i.e., the distance between minimum and maximum of the free energy landscape, may change.

hight of this barrier determines the rate coefficient $k_0$ for thermally activated spontaneous dissociation,

$$k_0 = \omega_0 \exp\left(-\beta \Delta G^{\ddagger}\right) . \tag{5}$$

Here, $\beta = 1/(k_B T)$ denotes the reciprocal thermal energy and $\omega_0$ the attempt frequency or Kramers' prefactor of the bound state[52–54]. For streptavidin/biotin dissociation, e.g., the reciprocal rate coefficient is several months, whereas it can be as short as milliseconds for antibody/antigen dissociation. Note that if unbinding is enforced at a time scale that is slower than the reciprocal rate coefficient, no dissociation force is measured, since in this case the system has fallen apart already before any significant force has been applied.

As is the force probe simulations described above, the force exerted by the cantilever is assumed harmonic and moving with velocity $v$,

$$V(x,t) = \tfrac{1}{2} k (x - vt)^2 , \tag{6}$$

(dashed curve in Fig. 6), where $k$ is the effective spring coefficient. Here we restrict our discussion to the case of small spring coefficients, i.e., soft springs, which covers most realistic situations. Therefore, $V(x,t)$ appears in the Figure as a nearly straight line, the slope of which increases linearly with time. Since the total potential $G(x) + V(x,t)$ now becomes time dependent, so does the barrier height $\Delta G^{\ddagger}$, and, hence, the dissociation coefficient $k_0$. This effect is demonstrated by the thin, solid lines. As can be seen, the barrier height decreases with time. Dissociation occurs when the barrier has become small enough to be overcome thermally activated at the time scale $\tau = \Delta G^{\ddagger}/(kv\Delta x)$ set by the loading rate $kv$.

For simple and localized barriers (left picture), we will neglect the slight shift of the position of the minimum that also occurs. In this case, a simple two-state model[47] is appropriate, which neglects the details of $G(x)$ and assumes a linear decrease of the barrier

height with time,

$$\Delta G^{\ddagger}(t) = \Delta G^{\ddagger} - kvt\Delta x\,. \tag{7}$$

This implies a time dependent dissociation coefficient [cf. eq. (5)],

$$k_0(t) = \omega_0 e^{-\beta(\Delta G^{\ddagger} - kvt\Delta x)}\,, \tag{8}$$

which holds as long as $\Delta G^{\ddagger} - kvt\Delta x$ is larger than $k_B T$ and back reactions can be neglected. In analogy to the treatment of radioactive decay, the flux across the barrier decreases the probability $P(t)$ to find the system in the bound state at time $t$,

$$\frac{dP(t)}{dt} = -P(t)k_0(t) = -P(t)\omega_0 e^{-\beta(\Delta G^{\ddagger} - kvt\Delta x)}\,, \tag{9}$$

with $P(t=0) = 1$. Solution of eq. (9),

$$P(t) = \exp\left[\frac{\omega_0}{\beta kv\Delta x} e^{-\beta\Delta G^{\ddagger}}\left(1 - e^{\beta kvt\Delta x}\right)\right]\,, \tag{10}$$

yields a distribution $p(t_D)dt_D = -\left.\frac{dP(t)}{dt}\right|_{t_D} dt_D$ of dissociation times $t_D$,

$$p(t_D)dt_D = \omega_0 e^{-\beta(\Delta G^{\ddagger} - kvt_D\Delta x)} \exp\left[\frac{\omega_0}{\beta kv\Delta x} e^{-\beta\Delta G^{\ddagger}}\left(1 - e^{\beta kvt_D\Delta x}\right)\right] dt_D\,, \tag{11}$$

and dissociation forces $F_D = kvt_D$, respectively,

$$p(F_D)dF_D = \omega_0 e^{-\beta(\Delta G^{\ddagger} - F_D\Delta x)} \exp\left[\frac{\omega_0}{\beta kv\Delta x} e^{-\beta\Delta G^{\ddagger}}\left(1 - e^{\beta F_D\Delta x}\right)\right] dF_D\,. \tag{12}$$

As the main result, the maximum ($dP(F_D)/dF_D = 0$) denoting the most probable dissociation force, reads

$$F_{\max}(v) = \frac{\Delta G^{\ddagger}}{\Delta x} + \frac{1}{\beta\Delta x}\ln\frac{\beta kv\Delta x}{\omega_0} = \frac{1}{\beta\Delta x}\ln\frac{\beta kv\Delta x}{k_0}\,, \tag{13}$$

(where eq. (5) has been used) and thus increases logarithmically with the loading rate $kv$.

This result links the rupture length $\Delta x$ to the slope of the loading rate dependent dissociation force and thus provides the basis for dynamic force spectroscopy (Fig. 7A) The larger $\Delta x$, the faster the energy barrier is decreased (cf. Fig. 6), and the stronger is the effect of the loading rate $kv$ on the dissociation time $t_D$ and dissociation force $F_D$. Furthermore, this result serves to rescale dissociation forces from force probe simulations to the much slower time scales of the AFM experiments.

For more complex energy landscapes as shown in Fig. 6 (right), the simple two-state model is not applicable. For the two barriers shown, there is a critical pulling force for which the left maximum becomes the global one (cf. the thin curve in the Figure) at the time of dissociation and, hence, the rupture length $\Delta x$ jumps to smaller values. Accordingly, the logarithmic slope of the dissociation force increases as shown in Fig. 7B. For a more general treatment, the reader is refereed to Refs. 50, 51.

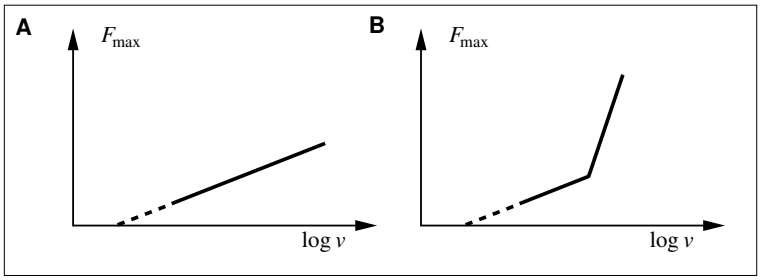


Figure 7. Dynamic force spectra show the increase of the dissociation force $F_{\max}$ with pulling velocity $v$ of the cantilever or, equivalently, loading rate $kv$. A: For the case of a well-localized energy barrier in $G(x)$, the simple two-state model described in the text predicts a logarithmic increase. B: For more complex energy landscapes such as the two barriers sketched in Fig. 6 (right), the dynamic force spectrum falls into two regimes. For small $v$, the larger barrier in $G(x)$ dominates, and the resulting large $\Delta x$ yields a slow increase of the spectrum with $v$. For large $v$, however, the (originally) smaller barrier to the left dominates at the time $t_D$ of dissociation, resulting in a steeper logarithmic increase of $F_{\max}$ with $v$.

## 7 Primary Mechanical Energy Transfer Steps in the "Molecular Nano-Machine" $F_1$ ATP Synthase [c]

As an example we consider force probe simulations that aim at elucidating the primary mechanical energy transfer steps in $F_1$ ATP synthase. In fact, this protein is the smallest rotary motor know to date.

The mitochondrial membrane protein $F_oF_1$-ATP synthase synthesizes adenosintriphosphate (ATP), the universal currency of energy in the cell. In the human body, about 70 kg of ATP are synthesized by these proteins each day. The protein (Fig. 8*a,b*) utilizes the electrochemical potential of a transmembrane proton gradient for ATP synthesis[55]. Remarkably, energy conversion involves mechano-chemical energy transport from a rotating asymmetric $\gamma$-"stalk" (red) over a distance of more than $2.5\,$nm to the three ATP synthesis sites of the protein (Fig. 8*a*)[56–58]. X-ray structures of the $F_1$-unit[59,60] show its three $\beta$-subunits in different conformational states, TP, DP, and E, with bound ATP (analog), ADP, and empty binding site, respectively[59]. The structures suggested that the energy consuming step in the ATP synthesis cycle, namely ATP release, is driven by concerted conformational motions within the $(\alpha\beta)_3$-complex, which are dictated by the changing orientation of the asymmetric $\gamma$-subunit inside $(\alpha\beta)_3$ (Ref. 59), thus rendering $F_oF_1$-ATP synthase a spectacular example of a "molecular machine".

Our molecular dynamics simulations included the $F_1$-unit, $(\alpha\beta)_3\gamma$ (except $\delta$ and b), bound nucleotides as shown in Fig. 8*a*, a large solvation shell (blue), and salt ions (red and yellow), comprising a total of $183\,674$ atoms. In the simulations, the lower part of the $\gamma$-stalk was enforced to rotate (Fig. 8*c*), thus resembling the rotation caused *in vivo* by protonmotive $F_o$-rotation, and the subsequently triggered conformational motions have been studied.

The $n$ backbone atoms of the lower part of the $\gamma$ subunit with positions $\mathbf{x}_i$ ($\bullet$) were

[c] This Section is adapted and shortened from Ref. 27.

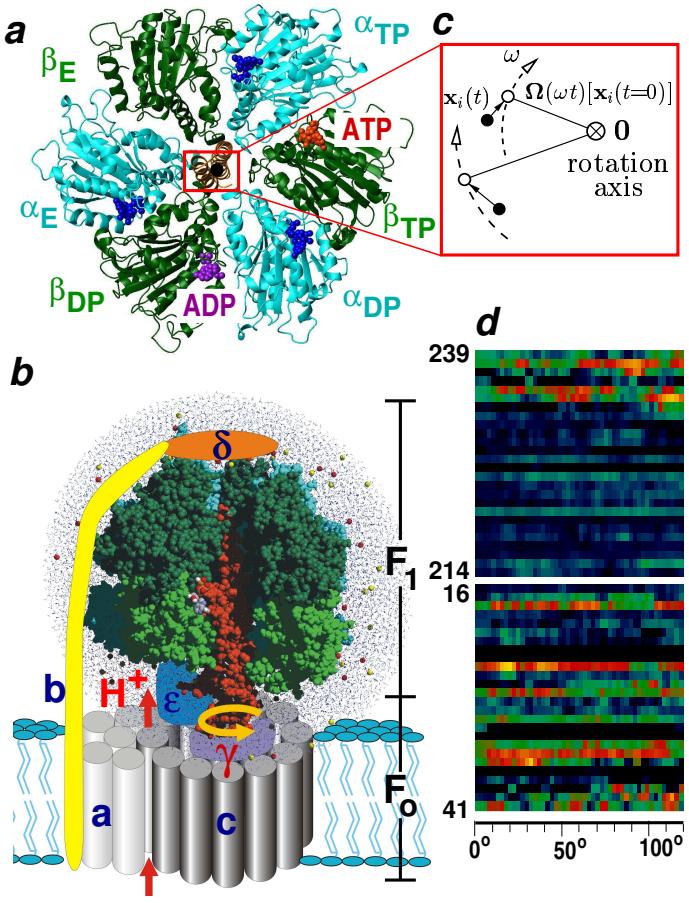


Figure 8. ATP synthase structure, function, and simulation setup. a: Slice through $F_1$ at the level of the active sites; b: $F_oF_1$-ATP synthase with the atomically resolved $F_1$ simulation system. A proton flux through the membrane-bound $F_o$-unit (red) drives rotation of the asymmetric $\gamma$-"stalk" (orange) with respect to the $F_1$-unit (green, cyan) located in the mitochondrial matrix; co-rotation of $F_1$ is hindered by $\delta$ and b (yellow). This rotation triggers conformational changes mainly within the three $\beta$-subunits, DP, TP, and E (green), which bind ADP and phosphate, and subsequently drive ATP synthesis and release. These changes concern most notably the orientation of the "lower half" of the $\beta$-subunit (light green), which can tilt with respect to the "upper half" (dark green). Accordingly, the conformation seen for the empty subunit, $\beta_{\mathrm{E}}$, is denoted "open", whereas $\beta_{\mathrm{TP}}$ and $\beta_{\mathrm{DP}}$ are referred to as "closed"[59]. After 120° rotation of $\gamma$, DP, TP, and E switch roles clockwise. c: In the simulations, a torque potential is used to enforce rotation of the $\gamma$ subunit (see text). d: The torque required to move the individual residues of $\gamma$ within $(\alpha\beta)_3$ (black: zero or negative torque; yellow: $0.7\times10^{-18}$ Nm) allows to identify "hot spots" of mechanical energy transfer.

subjected to a rotating potential,

$$V = \tfrac{1}{2}k\sum_{i=1}^{n}[\mathbf{\Omega}(\omega t)\mathbf{x}_i(t{=}0) - \mathbf{x}_i(t)]^2. \tag{14}$$

The rotation matrix $\mathbf{\Omega}$ moved the minima of $V$ ($\circ$) along concentric circles around the

symmetry axis of the complex, using a stiff spring coefficient $k$. The torques $\mathbf{\Theta}_i(t)$ exerted on the individual atoms were computed from the deflection of the actual atomic positions $\mathbf{x}_i(t)$ from the respective minima,

$$\mathbf{\Theta}_i(t) = \mathbf{\Omega}(\omega t)\mathbf{x}_i(t{=}0) \times k[\mathbf{\Omega}(\omega t)\mathbf{x}_i(t{=}0) - \mathbf{x}_i(t)]\,. \tag{15}$$

Throughout the simulations, co-rotation of the $(\alpha\beta)_3$-complex was prevented by immobilizing the centers of mass of the putative $\delta$ contact region of two $\alpha$-subunit head groups, thereby mimicking the effect of the $\delta$ "stator".

With this approach we studied how the rotating $\gamma$-stalk induces conformational motions within the $\beta$ subunits, how and along which route they propagate towards the nucleotide binding sites, and why and in what sequence the observed structural changes lower ATP binding affinity at $\beta_{\mathrm{TP}}$, as is required for ATP to leave the binding pocket after synthesis.

Due to the huge computational cost of such simulations, the covered time span is limited to several nanoseconds, i.e., considerably shorter than the microseconds time scale at which the studied conformational motions likely take place *in vivo*[61]. Accordingly, torques that are larger by factors of 12 and 50, respectively, than the measured ones[62] had to be applied in the simulations. Furthermore, slow (microsecond) conformational motions are unlikely to show up. For the faster motions that are actually seen in the simulations, however, the large amount of available experimental data enabled to assure that these motions are actually described correctly.

After equilibration, a $120^{\mathrm{o}}$ force probe rotation simulation in synthesis direction was carried out with an angular velocity of $\omega = 115^{\mathrm{o}}\,\mathrm{ns}^{-1}$, as sketched in Fig. 8*c*. During a subsequent relaxation period of $3.5$ ns, within which the lower part of the $\gamma$-subunit was kept restrained to avoid back-rotation, the induced conformational motions propagated further towards the active sites. The torques exerted onto the individual $\gamma$-residues during the $120^{\mathrm{o}}$ enforced rotation (Fig. 8*d*) show peaks, reflecting energy transfer to $(\alpha\beta)_3$, dissipation, and enforced crossing of associated energy barriers.

Figure 9 shows the main changes for $\beta_{\mathrm{TP}}$, $\beta_{\mathrm{E}}$, and $\beta_{\mathrm{DP}}$ during enforced rotation and subsequent free dynamics. The lower part of $\beta_{\mathrm{TP}}$ is pushed sidewards towards $\alpha_{\mathrm{DP}}$, and downwards towards an open configuration (Fig. 9*b*). This observation is quantified by the change of the bending angle (inset) between the two domains separated by the dashed line in Fig. 9*a*, which approaches the one seen in $\beta_{\mathrm{E}}$.

Simultaneously, an upwards rotation of the $\beta_{\mathrm{E}}$ lower half towards the closed x-ray conformation of $\beta_{\mathrm{TP}}$ and $\beta_{\mathrm{DP}}$ is observed (Fig. 9*c*). This motion is initially sterically obstructed by both the $\gamma$-subunit and $\beta_{\mathrm{TP}}$ and, therefore, proceeds synchronously to the removal of these obstacles. Much less changes are seen for $\beta_{\mathrm{DP}}$ (*d*), where the orientation of the lower part is nearly unchanged. Overall, the opening and closing motions of the lower halves of the $\beta$-subunits are nearly completed already within the 7 ns simulation time span without explicitly being forced to.

Focusing at the catalytic ATP binding site (Fig. 10), a sequential retraction of $\beta$Arg 191, $\alpha$Arg 373, and $\beta$Arg 189 from ATP is seen, quantified by the respective distance changes (inset, blue curves). This sequence is initiated, immediately after $\gamma$-rotation, by a $0.5$ nm shift of $\beta$Arg 191 towards $\alpha_{\mathrm{TP}}$, which forms a new hydrogen bond to $\alpha$Gln 163, thereby weakening its interaction to ATP. Subsequently, initially strong hydrogen bonds (dashed lines) between ATP and residues $\alpha$Arg 373 and $\beta$Arg 189 rupture, thus further decreasing ATP binding affinity. The whole process is compatible with the "zipper-model"[63]. Assum-

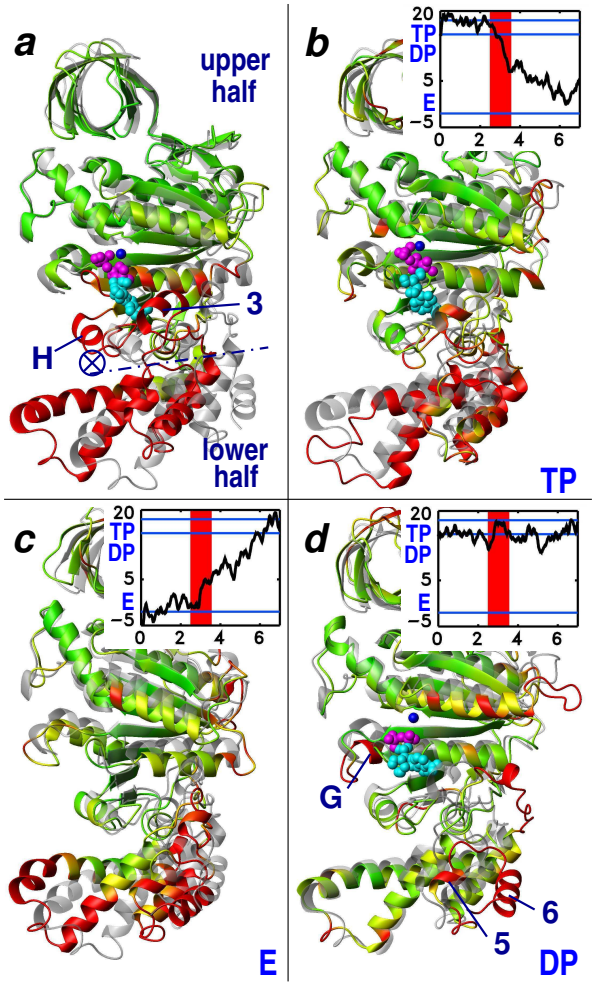


Figure 9. Structural changes of the $\beta$-subunits induced by enforced rotation of the $\gamma$-stalk. The size of these changes is color coded (green: small; red: large). a: Overlay of $\beta_{\mathrm{TP}}$ (colored) and $\beta_{\mathrm{E}}$-subunits (grey) taken from the x-ray structure, which are in closed and open conformation, respectively. b–d: Changes in $\beta_{\mathrm{TP}}$, $\beta_{\mathrm{E}}$, and $\beta_{\mathrm{DP}}$, as induced by enforced 120° rotation and subsequent free dynamics; shown are initial (x-ray) structures (grey) and final structures (colored). The insets show the angle between upper and lower part of the respective $\beta$-subunits in the course of the 7 ns simulation (axis: $\otimes$). The red bar indicates the period of enforced rotation, green lines denote the three $\beta$-subunit angles of the equilibrated x-ray structure.

ing that changes of ATP binding affinity are dominated by the interaction between ATP and the binding pocket, a continuous ATP affinity decrease of $\beta_{\mathrm{TP}}$ can be inferred from the increasing interaction energy estimate between ATP and the binding pocket (inset, black curve) as the net effect of the observed structural changes.

Taken together, the enforced $\gamma$-rotation suggests for this beautiful molecular machine a sequence of structural changes that effect primary mechano-chemical energy transfer steps within $F_1$-ATP synthase. Many structural changes that are expected from the three

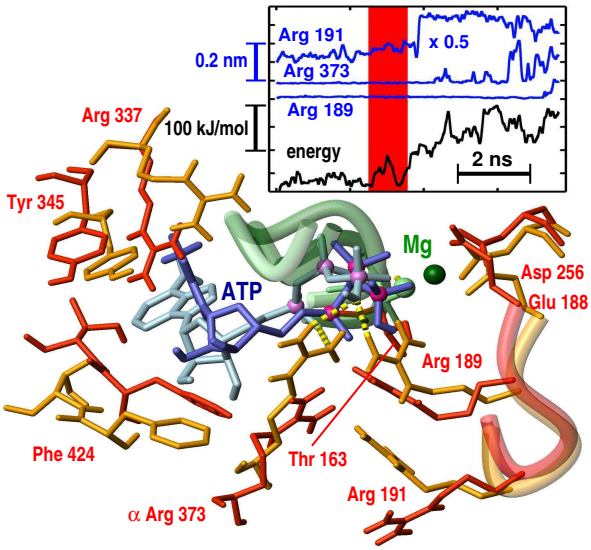


Figure 10. Changes at the $\beta_{\mathrm{TP}}$ ATP binding site after the 120° and free dynamics. Shown are selected residues involved in ATP binding before (yellow, ATP in light blue) and after enforced rotation and subsequent free dynamics (red, ATP in blue). The backbones of part of the P-loop and of are colored green and orange, respectively. Residue numbers refer to $\beta_{\mathrm{TP}}$ if not annotated otherwise. The inset shows distances (blue) between the donor nitrogen atoms of three arginine residues involved in ATP binding and the respective ATP phosphates (reduced scale for Arg 191), as well as an estimate (black) for the change in interaction energy between ATP and the binding pocket in the course of the simulation. The period of enforced rotation is highlighted red.

x-ray intermediates are correctly reproduced. Because none of these motions have been artificially directed towards the expected target structure, the agreement shows that the necessarily accelerated rotation of the $\gamma$-stalk does not severely change their character.

Moreover, the simulations provide a *causal* picture of a sequence of structural motions, one triggering the next. Already within the simulation time span of 7 ns, the structural changes proceed sufficiently far to transfer a significant amount of energy to the $\beta_{\mathrm{TP}}$ binding site, as estimated from its decreased ATP binding affinity. This decrease is affected gradually, by sequential and well concerted retraction of three charged arginines from the bound ATP.

## Acknowledgments

I would like to thank Berthold Heymann and Rainer Böckmann for their contributions which are presented here.

## References

1. Jeremy M. Berg, John L. Tymoczko, and Lubert Stryer. *Biochemistry*. W. H. Freeman and Company, New York, 2002.

2. Ken A. Dill and Sarina Bromberg. *Molecular Driving Forces: Statistical Thermodynamics in Chemistry and Biology*. Garland Publishing, London, 2003.
3. Thomas E. Creighton. Protein folding. *Biochem. J.*, 270:1–16, 1990.
4. F. C. Bernstein, T. F. Koetzle, G. J. B. Williams, E. F. Meyer, M. D. Brice, J. R. Rodgers, O. Kennard, T. Shimanouchi, and M. J. Tasumi. The protein data bank: A computer-based archival file for molecular structures. *J. Molec. Biol.*, 112:535–542, 1977.
5. J. C. Kendrew, G. Bodo, H. N. Dintzis, R. G. Parrish, H. Wyckoff, and D. C. Phillips. 3-dimensional model of the myoglobin molecule obtained by x-ray analysis. *Nature*, 181:662–666, 1958.
6. A. Ansari, J. Berendzen, S. F. Browne, H. Frauenfelder, I. E. T. Iben, T. B. Sauke, E. Shyamsunder, and R. D. Young. Protein states and protein quakes. *Proc. Natl. Acad. Sci. USA*, 82:5000–5004, 1985.
7. Erwin Neher and Bert Sakmann. Single-channel currents recorded from membrane of denervated frog muscle fibres. *Nature*, 260:799–802, 1976.
8. Bert Sakmann and Erwin Neher, editors. *Single-Channel Recording*. Plenum Press, 2nd edition, 1995.
9. Gary Yellen. The voltage-gated potassium channels and their relatives. *Nature*, 419:35–42, 2002.
10. Anjum Ansari, Joel Berendzen, David Braunstein, Benjamin R. Cowen, Hans Frauenfelder, Mi Kyung Hong, Icko E. T. Iben, J. Bruce Johnson, Pál Ormos, Todd B. Sauke, Reinhard Scholl, Alfons Schulte, Peter J. Steinbach, Joseph Vittitow, and Robert D. Young. Rebinding and relaxation in the myoglobin pocket. *Biophys. Chem.*, 26:337–355, 1987.
11. R. Elber and M. Karplus. Multiple conformational states of proteins: A molecular dynamics analysis of myoglobin. *Science*, 235:318–321, 1987.
12. H. J. C. Berendsen. Bio-molecular dynamics comes of age. *Science*, 271:954–955, 1996.
13. E. Fermi, J. Pasta, and S. Ulam. Studies in nonlinear problems, I. Los Alamos Report LA 1940, 1955.
14. B. J. Alder and T. E. Wainwright. Phase transition for a hard sphere system. *J. Chem. Phys.*, 27:1208–1209, 1957.
15. A. Rahman. Correlations in the motion of atoms in liquid argon. *Phys. Rev.*, 136:A405–A411, 1964.
16. Loup Verlet. Computer "experiments" on classical fluids. I. Thermodynamical properties of Lennard-Jones molecules. *Phys. Rev.*, 159:98–103, 1967.
17. A. Rahman and F. H. Stillinger. Molecular dynamics study of liquid water. *J. Chem. Phys.*, 55:3336–3359, 1971.
18. M. Karplus, R. N. Porter, and R. D. Sharme. Exchange reactions with activation energy. I. Simple barrier potential for (H, $H_2$). *J. Chem. Phys.*, 43:3259–3287, 1965.
19. H. A. Scheraga, R. A. Scott, and K. D. Gibson. Calculations of stable polypeptide conformations. *Fed. Proc.*, 25:345, 1966.
20. M. Levitt and Shneior Lifson. Refinement of protein conformation using a macromolecular energy minimization procedure. *J. Molec. Biol.*, 46:269–279, 1969.
21. J. A. McCammon, B. R. Gelin, and M. Karplus. Dynamics of folded proteins. *Nature*, 267:585–590, 1977.

22. W. F. van Gunsteren and H. J. C. Berendsen. Algorithms for macromolecular dynamics and constraint dynamics. *Molec. Phys.*, 34:1311–1327, 1977.
23. M. Karplus and J. A. McCammon. The dynamics of proteins. *Scient. Am.*, 4:30, 1986.
24. Y. Duan and P. A. Kollman. Pathways to a protein folding intermediate observed in a 1-microsecond simulation in aqueous solution. *Science*, 282:740–744, 1998.
25. Christopher D. Snow, Houbi Nguyen, Vijay S. Pande, and Martin Gruebele. Absolute comparison of simulated and experimental protein-folding dynamics. *Nature*, 420:102–106, 2002.
26. Bert L. de Groot and Helmut Grubmüller. Water permeation across biological membranes: Mechanism and dynamics of aquaporin-1 and GlpF. *Science*, 294:2353–2357, 2001.
27. Rainer Böckmann and Helmut Grubmüller. Nanoseconds molecular dynamics simulation of primary mechanical energy transfer steps in $F_1$-ATP synthase. *Nature Struct. Biol.*, 9:198–202, 2002.
28. L. Pauling, R. B. Corey, and H. R. Branson. The structure of proteins: Two hydrogen-bonded helical configurations of polypeptide chain. *Proc. Natl. Acad. Sci. USA*, 37:205, 1951.
29. Gunnar Schröder. Molekulardynamiksimulation der Flexibilität und Fluoreszenzanisotropie eines an ein Protein gebundenen Farbstoffs. Master's thesis, Universität Göttingen, 2000.
30. Wilfred F. van Gunsteren and Herman J. C. Berendsen. Computer simulation of molecular dynamics: Methodology, applications, and perspectives in chemistry. *Angew. Chem. Int. Ed.*, 29:992–1023, 1990.
31. M. Parrinello. Simulating complex systems without adjustable parameters. *IEEE Computational Science & Engineering*, 2:22–27, 2000.
32. M. E. Tuckerman and G. J. Martyna. Understanding modern molecular dynamics: Techniques and applications. *J. Phys. Chem. B*, 104:159–178, 2000.
33. Wilfred F. van Gunsteren, Paul K. Weiner, and Anthony J. Wilkinson, editors. *Computer Simulation of Biomolecular Systems: Theoretical and experimiental applications*, volume 1-3. Escom, Leiden, The Netherlands, 1989–1997.
34. Helmut Grubmüller. Computersimulation der Dynamik von Biomolekülen. Book Chapter for Bergmann/Schaefer, Lehrbuch der Experimentalphysik, Band 5: Vielteilchensysteme. In press.
35. Matthias Rief and Helmut Grubmüller. Kraftspektroskopie von einzelnen Biomolekülen. *Physikalische Blätter*, pages 55–61, Feb. 2001.
36. J. T. Finer, R. M. Simmons, and J. A. Spudich. Single myosin molecule mechanics: piconewton forces and nanometer steps. *Nature*, 368:113–119, 1994.
37. H. Yin, M. D. Wang, K. Svoboda, R. Landick, S. M. Block, and J. Gelles. Transcription against an applied force. *Science*, 270:1653–1657, 1995.
38. Helmut Grubmüller, Berthold Heymann, and Paul Tavan. Ligand binding: Molecular mechanics calculation of the streptavidin-biotin rupture force. *Science*, 271:997–999, 1996.
39. S. Izrailev, S. Stepaniants, M. Balsera, Y. Oono, and K. Schulten. Molecular dynamics study of unbinding of the avidin-biotin complex. *Biophys. J.*, 72:1568–1581, 1997.
40. H. Lu, B. Isralewitz, A. Krammer, V. Vogel, and K. Schulten. Unfolding of titin

immunoglobulin domains by steered molecular dynamics simulation. *Biophys. J.*, 75:662–671, 1998.
41. P. Marszalek, H. Lu, H. Li, M. Carrion-Vazquez, A. F. Oberhauser, K. Schulten, and J. M. Fernandez. Mechanical unfolding intermediates in titin modules. *Nature*, 402:100–103, 1999.
42. Matthias Rief, Filipp Oesterhelt, Berthold Heymann, and Hermann E. Gaub. Single molecule force spectroscopy reveals conformational change in polysaccharides. *Science*, 275:1295–1297, 1997.
43. A. D. MacKerell and G. U. Lee. Structure, force, and energy of a double-stranded DNA oligonucleotide under tensile loads. *Europ. Biophys. J.*, 28:415–426, 1999.
44. Berthold Heymann and Helmut Grubmüller. Elastic properties of poly(ethyleneglycol) studied by molecular dynamics stretching simulations. *Chem. Phys. Lett.*, 307:425–432, 1999.
45. B. Isralewitz, M. Gao, and K. Schulten. Steered molecular dynamics and mechanical functions of proteins. *Curr. Opin. Struct. Biol.*, 11:224–230, 2001.
46. Helmut Grubmüller. Kraftmikroskopische Experimente an einzelnen Biomolekülen. Book Chapter for Bergmann/Schaefer, Lehrbuch der Experimentalphysik, Band 5: Vielteilchensysteme. In press.
47. G. I. Bell. Models for specific adhesion of cells to cells. *Science*, 200:618–627, 1978.
48. Evan Evans and Ken Ritchie. Dynamic strength of molecular adhesion bonds. *Biophys. J.*, 72:1541–1555, 1997.
49. U. Seifert. Rupture of multiple parallel molecular bonds under dynamic loading. *Phys. Rev. Lett.*, 84:2750–2753, 2000.
50. Berthold Heymann and Helmut Grubmüller. Dynamic force spectroscopy of molecular adhesion bonds. *Phys. Rev. Lett.*, 84:6126–6129, 2000.
51. G. Hummer and A. Szabo. Kinetics from nonequilibrium single-molecule pulling experiments. *Biophys. J.*, 85:5–15, 2003.
52. H. Eyring. The activated complex in chemical reactions. *J. Chem. Phys.*, 3:107–115, 1935.
53. H. A. Kramers. Brownian motion in a field of force and the diffusion model of chemical reactions. *Physica (Utrecht)*, VII:284–304, 1940.
54. Peter Hänggi, Peter Talkner, and Michal Borkovec. Reaction-rate theory: Fifty years after Kramers. *Rev. Mod. Phys.*, 62:251–341, Apr. 1990.
55. P. D. Boyer. The binding change mechanism for ATP synthase — some probabilities and possibilities. *Biochim. Biophys. Acta*, 1140:215–250, 1993.
56. T. M. Duncan, V. V. Bulygin, Y. Zhou, M. L. Hutcheon, and R. L. Cross. Rotation of subunits during catalysis by Escherichia-coli $F_1$-ATPase. *Proc. Natl. Acad. Sci. USA*, 92:10964–10968, 1995.
57. D. Sabbert, S. Engelbrecht, and W. Junge. Intersubunit rotation in active F-ATPase. *Nature*, 381:623– 625, 1996.
58. H. Noji, R. Yasuda, M. Yoshida, and K. Kinosita. Direct observation of the rotation of $F_1$-ATPase. *Nature*, 386:299–302, 1997.
59. Jan Pieter Abrahams, Andrew G. W. Leslie, René Lutter, and John E. Walker. Structure at $2.8\,$Å resolution of $F_1$-ATPase from bovine heart mitochondria. *Nature*, 370:621–628, 1994.
60. C. Gibbons, M. G. Montgomery, A. G. W. Leslie, and J. E. Walker. The structure

of the central stalk in bovine $F_1$-ATPase at 2.4 å resolution. *Nature Struct. Biol.*, 7:1055–1061, 2000.

61. R. Yasuda, H. Noji, M. Yoshida, K. Kinoshita, and H. Itoh. Resolution of distinct rotational substeps by submillisecond kinetic analysis of $F_1$-ATPase. *Nature*, 410:898–904, 2001.
62. O. Pänke, D. A. Cherepanov, K. Gumbiowski, S. Engelbrecht, and W. Junge. Viscoelastic dynamics of actin filaments coupled to rotary F-ATPase: Angular torque profile of the enzym. *Biophys. J.*, 81:1220–1233, 2001.
63. G. Oster and H. Y. Wang. Reverse engineering a protein: the mechanochemistry of ATP synthase. *Biochim. Biophys. Acta*, 1458:482–510, 2000.